Surface-Modified Metallic $Ti_3C_2T_x$ MXene as Electron Transport Layer for Planar Heterojunction Perovskite Solar Cells

Lin Yang, Chunxiang Dall'Agnese, Yohan Dall'Agnese, Gang Chen, Yu Gao, Yoshitaka Sanehira, Ajay Kumar Jena, Xiao-Feng Wang, Yury Gogotsi and Tsutomu Miyasaka*

L. Yang, Dr. C. Dall'Agnese, Prof. G. Chen, Prof. Y. Gao, Prof. X.-F. Wang, Prof. Y. Gogotsi

Key Laboratory of Physics and Technology for Advanced Batteries (Ministry of Education), College of Physics, Jilin University, 2699 Qianjin Street, Changchun 130012, China

E-mail: xf_wang@jlu.edu.cn

Prof. Y. Dall'Agnese

Institute for Materials Discovery, University College London, London WC1E 7JE, United Kingdom

Prof. Y. Gogotsi

A. J. Drexel Nanomaterials Institute, and Department of Materials Science and Engineering, Drexel University, Philadelphia, Pennsylvania 19104, United States

Dr. Y. Sanehira, Dr. A. K. Jena, Prof. T. Miyasaka

Graduate School of Engineering, Toin University of Yokohama, 1614 Kurogane-cho, Aoba, Yokohama, Kanagawa 225-8503, Japan

Keywords: UV-ozone treatment, $Ti_3C_2T_x$ MXene, electron transport layers, perovskite solar cells

MXenes are a large and rapidly expanding family of two-dimensional (2D) materials which, owing to their unique optoelectronic properties and tunable surface termination, find a wide range of applications including energy storage and energy conversion. In this work, $Ti_3C_2T_x$ MXene nanosheets are applied as a novel type of electron transport layer (ETL) in low-temperature processed planar-structured perovskite solar cells (PSCs). Interestingly, simple UV-ozone treatment of the metallic $Ti_3C_2T_x$ that increases the surface Ti-O bonds without any change in its bulk properties like high electron mobility improves its suitability as an ETL. Improved electron transfer and suppressed recombination at the ETL/perovskite interface results in augmentation of the power conversion efficiency (PCE) from 5.00% in the case of $Ti_3C_2T_x$ without UV-ozone treatment to the champion PCE of 17.17%, achieved using the $Ti_3C_2T_x$ film after 30 minutes of UV-ozone treatment. As the first report on the use of pure MXene layer as an ETL in PSCs, this work shows great potential of MXenes to be used in PSCs and displays their promises for applications in photovoltaic technology in general.

1. Introduction

Since methylammonium lead iodide ($CH_3NH_3PbI_3$) was first reported by Miyasaka *et al.* in 2009 as a light absorbing material for emerging technology of the third generation photovoltaics,[1] organic-inorganic lead halide perovskite solar cells (PSCs) have gained enormous attention over the past decade.[2] Appropriate bandgap, high absorption coefficient, long carrier diffusion length, and high charge carrier mobility have made hybrid perovskites emerge as efficient and low-costmaterials for photovoltaic applications.[3] PSCs have witnessed a rapid development of the power conversion efficiency (PCE), rising from 3.8% to above 24%,[4] getting closer and closer to the theoretical efficiency of 33.5%.[5]

It's well known that the ETL is an essential architectural component of efficient PSCs, which plays an important role in suppressing charge recombination and rectifying photocurrent.[6] Therefore, the exploration of efficient materials for ETLs remains one of the challenging issues.[7] There are highly efficient PSCs based on meso-superstructured TiO_2, but high-temperature sintering above 450 °C limits their practical applications in scalable and flexible devices.[8] TiO_x layers prepared by low-temperature methods have recently gained much attraction,[9] especially aiming at flexible PSCs. In general, efforts have been made to increase the conductivity metal oxide ETLs like TiO_2 and SnO_2 for efficient carrier transfer and thus, higher efficiency. Use of 2D materilas like graphene has been found to improve efficiency of PSCs. For example, graphene/TiO_2 used as an ETL by Wang *et al.* has resulted in a PCE of 15.6%.[10] Reduced graphene oxide (rGO) has also been proven effective in improving the conductivity of GO and Jokar *et al.* have reported rGO-based inverted PSC with a PCE of 16%.[11] Singh *et al.* explored MoS_2 as ETL and achieved a PCE of 13.14%.[12] Lu *et al.* delivered a successful synthesis of few-layered bismuthene, which exhibits great potential in photonics devices.[13] These studies have demonstrated the great potential of conductive 2D materials for application in PSCs.

MXenes are 2D transition metal carbides and nitrides with a composition of $M_{n+1}X_nT_x$, where M represents an early transition metal, X indicates carbon and/or nitrogen, and T_x is the surface termination groups (usually -O, -OH and/or -F).[14] $Ti_3C_2T_x$ as the first discovered and most widely studied MXene has shown outstanding performance in lithium-ion batteries,[15] supercapacitors,[16] sensors,[17] and antennas [18] due to its high electrical conductivity, flexibility, and hydrophilicity that enables processing from aqueous

solutions.[19] In addition, $Ti_3C_2T_x$ has been applied in dye-sensitized solar cells [20] and as an additive in perovskite layer or SnO_2 ETL for perovskite solar cells.[21] Zhou *et al.* presented a systematic computational study of interlayer-decoupled Sc-based MXene with carrier mobilities of about $1- 4.5 \times 10^4$ cm^2 V^{-1} s^{-1} and strong light-harvesting ability.[22] Recently, Fu *et al.* demonstrated delaminated few layered $Ti_3C_2T_x$ MXene contacted Si solar cells with a maximum PCE of ≈11.5%.[23] Yu *et al.* tried $Ti_3C_2T_x$ as electron- and hole-transport layers in organic solar cells and achieved a PCE of 9.06%.[24] Yet, the applications of MXenes in solar cells remain almost unexplored. $Ti_3C_2T_x$ has metallic character of conductivity, promising photonic properties, and oxide-like surface termination that can be tuned to exhibit suitable properties as ETL for PSCs.[25] The potential use of $Ti_3C_2T_x$ as ETL to replace traditional semiconductor materials in PSCs greatly intrigued us.

In this work, $Ti_3C_2T_x$ nanosheets were prepared as ETL by spin-coating colloidal solutions onto indium tin oxide (ITO) substrates for the low-temperature processed planar PSCs. UV-ozone treatment was applied to the surface of $Ti_3C_2T_x$ films, and devices with an architecture of ITO/$Ti_3C_2T_x$/$CH_3NH_3PbI_3$/Spiro-OMeTAD/Ag were fabricated. The results reveal that the optimum time of UV-ozone treatment of the $Ti_3C_2T_x$ film can generate oxide-like Ti-O bonds,[25b] rendering it suitable as ETL for PSCsby improving the interface properties of the $Ti_3C_2T_x$/perovskite junction.[26] The devices fabricated with the UV-ozone treated $Ti_3C_2T_x$ showed an increase in short-circuit current density (J_{sc}), open-circuit voltage (V_{oc}) and fill factor (FF), resulting in much higher PCE than those without the UV-ozone treatment. The pristine $Ti_3C_2T_x$-based device achieved a PCE of 5.00%, while the champion PCE of 17.17% was demonstrated by the device with 30 min UV-ozone-treated $Ti_3C_2T_x$ film.

The improvement of PCE can be attributed to the additional Ti-O bonds in $Ti_3C_2T_x$ induced by UV-ozone treatment, which facilitate electron transfer and prevent their recombination at the $Ti_3C_2T_x$ /perovskite interface.

2. Results and Discussion

2.1. Characterization of $Ti_3C_2T_x$ nanosheets and UV-ozone treated $Ti_3C_2T_x$ films

The $Ti_3C_2T_x$ MXene nanosheets were synthesized by etching the Al layers from Ti_3AlC_2 MAX phase and exfoliating the layers according to the minimally intensive layer delamination method (MILD),[14b] as represented in **Figure 1**a. Figure 1b shows the X-ray diffraction (XRD) patterns of Ti_3AlC_2 before and after 24 hours of etching. Disappearance of the most intense peak of Ti_3AlC_2 (104) at 38.9° (2θ) and the shift of the (002) peak from 9.5° to about 7°indicates the topochemical synthesis of $Ti_3C_2T_x$. The corresponding scanning electron microscopy (SEM) images (Figure 1c) show the compacted ceramic structure before etching Al layer and single/few layered nanosheets after etching. (Figure 1d)

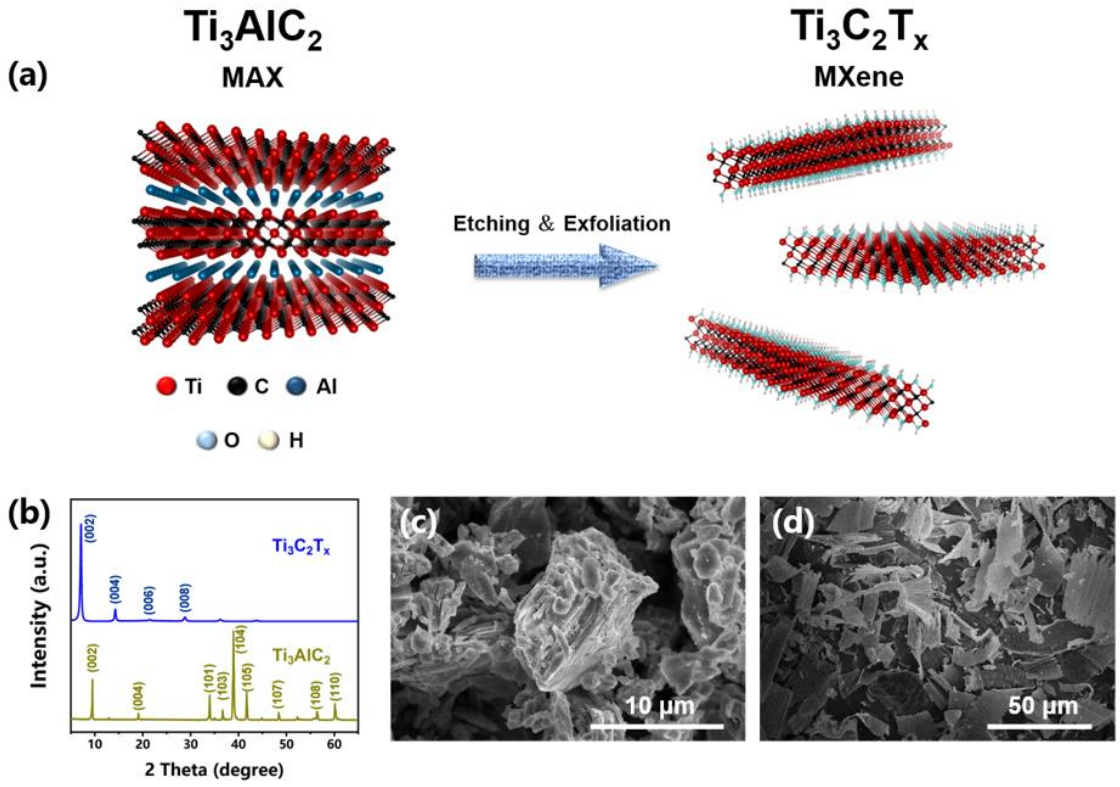

Figure 1. (a) Schematic representation of $Ti_3C_2T_x$ synthesis. (b) XRD patterns of Ti_3AlC_2 powder and dried $Ti_3C_2T_x$ film. Top-view SEM images of (c) Ti_3AlC_2 powder and (d) $Ti_3C_2T_x$ nanosheets.

As illustrated in **Figure 2**a, spin-coating of $Ti_3C_2T_x$ colloidal dispersion (1 mg mL^{-1}) onto ITO, then UV-ozone treatments for different times (0, 10, 30, or 60 min) were carried out for preparation of the ETLs. Figures 2b-2e show the SEM images of $Ti_3C_2T_x$ nanosheets coated on the ITO substrates treated by UV-ozonation for different times. As can be seen in the figures, there was no noticeable difference between films before and after UV-ozone treatment. The XRD patterns (Figure 2f) and the UV-vis absorption spectra (Figure 2g) of these films are also in accordance with the SEM images, showing no difference in crystal

structure and morphology. Moreover, transmission electron microscopy (TEM) (**Figure S1**) and Raman spectroscopy (**Figure S2**) of $Ti_3C_2T_x$ films before and after UV-ozone treatment also corresponded to it. These indicate that neither oxidization nor other reactions of $Ti_3C_2T_x$ films occurred during UV-ozone treatment. Indeed, this is not surprising because the role of UV-ozone is supposed to only desorb functional groups, increase hydrophilicity of the film and improve the interface properties of $Ti_3C_2T_x$/perovskite.[26]

In order to check the functionality of $Ti_3C_2T_x$ as an ETL and effect of UV-ozone treatment of the film on photovoltaic performance of PSCs, devices of planar architecture (ITO/ETL/$CH_3NH_3PbI_3$/Spiro-OMeTAD/Ag) were fabricated. The flatness and uniformity of the $Ti_3C_2T_x$ films (shown in **Figures S3**a-3d) suggests that the PSCs are planar-heterojunction type solar cells.

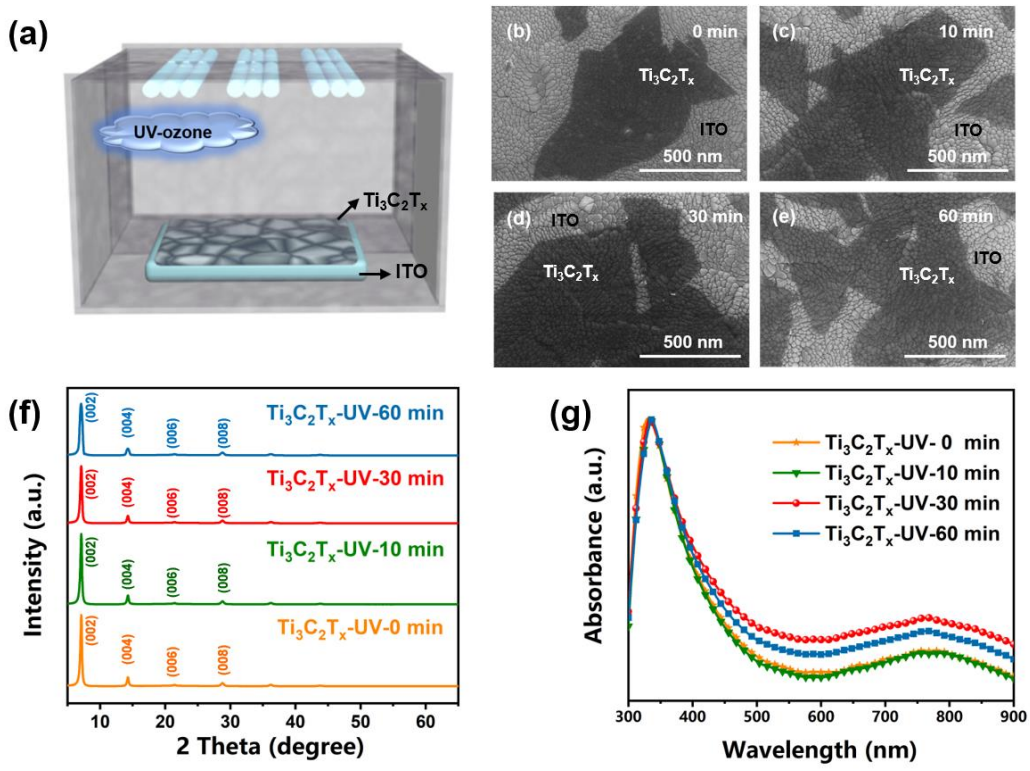

Figure 2. (a) Schematic representation of UV-ozone treatment on $Ti_3C_2T_x$ film fabricated by spin-coating, (b-e) SEM images, (f) XRD patterns and (g) UV-vis absorption spectra of pristine $Ti_3C_2T_x$ film and $Ti_3C_2T_x$ films treated by UV-ozone for 10, 30, and 60 min, respectively.

Chemical changes of $Ti_3C_2T_x$ MXene film arisen from UV-ozone treatment were studied by X-ray photoelectron spectroscopy (XPS), as shown in **Figure 3** and **Figure S4**, which is a direct and powerful method to get insight into the bonding of samples. From Figures S4a-4d, the peaks belonging to Ti, C, O, F were clearly detected. In the high-resolution XPS spectrum of Ti 2p (Figure 3), the doublet at 454.8 eV and 460.8 eV stems from Ti-C bond (blue), and the doublet at 458.3 eV and 464.3 eV stems from Ti-O bond (green), while the doublet of Ti-T_x at 456.8 eV and 462.6 eV is the combinations of Ti-F bond and Ti-OH bond.[27] The changes in Ti-C bond, Ti-O bond and Ti-T_x bond suggest a change in the surface termination groups before and after UV-ozone treatment. By comparing the fitting results, a significant increase in the ratio of Ti-O bond at 458.3 eV and 464.4 eV was found, suggesting the UV-ozone treatment induced the film of $Ti_3C_2T_x$ to form more Ti-O bond. With the increasing time of UV-ozone treatment, more Ti-O bonds were formed on the surface of $Ti_3C_2T_x$, achieving the maximum value after 30 min treatment. Then there was no more Ti-O bond addition with longer treatment of UV-ozone, as shown in Figures 3b-3d. As the SEM images and XRD patterns shown in Figures 2b-2f, there was no difference in the film morphology and structure before and after UV-ozone treatment, meaning no oxide formation occurred during the treatment. Thus, the newly formed Ti-O bond of $Ti_3C_2T_x$ film did not arise from the oxide product (TiO_2), it is just a kind of oxide-like surface termination formed

on the surface of the film.

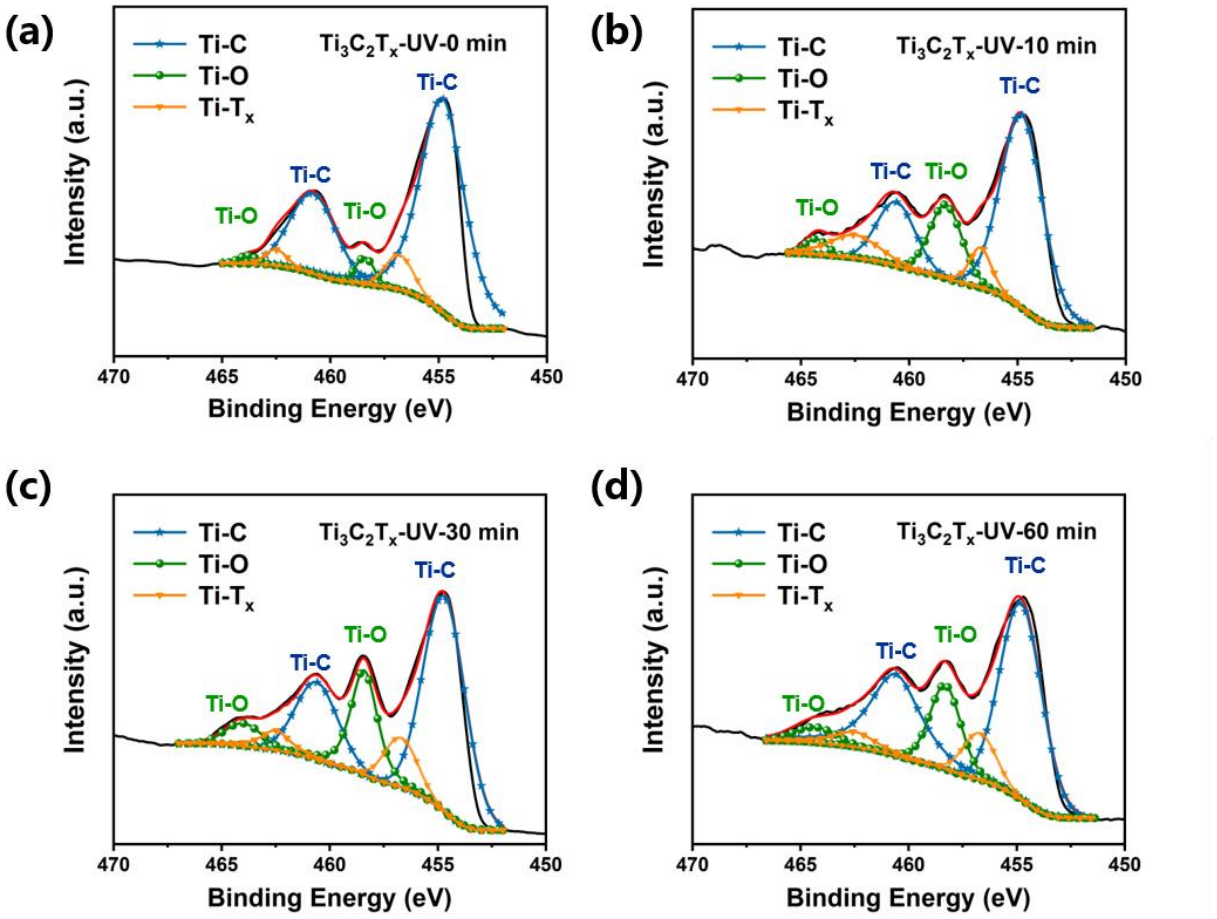

Figure 3. Ti 2p core level XPS spectra of (a) $Ti_3C_2T_x$ film and (b-d) films treated with UV-ozone for 10, 30 and 60 min, respectively.

2.2. Photovoltaic characterization

In order to determine the performance of $Ti_3C_2T_x$ MXene before and after UV-ozone treatment working as the ETL in PSCs, the devices with an architecture of ITO/ETL/$CH_3NH_3PbI_3$/Spiro-OMeTAD/Ag were fabricated (**Figure 4**a). Figure 4b shows a typical cross-sectional SEM image of the planar PSC device made with a thin $Ti_3C_2T_x$ layer as an ETL. The cross-sectional SEM image of $Ti_3C_2T_x$ layer and perovskite is shown in

Figure S5, from which the thickness of $Ti_3C_2T_x$ layer is obtained to be 18 ± 3 nm. Figure 4c shows the schematic energy-level diagram of each component in the PSC device, where the work functions are determined by extracting 25 points using a Kelvin probe system (see **Figure S6**). The work function of $Ti_3C_2T_x$ has an obvious shift from -5.52eV to -5.62eV after UV-ozone treatment, making it more suitable for electron transporting. The current density-voltage (*J-V*) curves of PSCs based on $Ti_3C_2T_x$ treated by UV-ozone for different times are given in Figure 4d and the Table 1 summarizes the corresponding photovoltaic parameters including J_{sc}, V_{oc}, FF and PCE. As can be seen from the data, the PCEs, J_{sc}, V_{oc}, and FF of the devices with UV-ozone treated $Ti_3C_2T_x$ films were remarkably higher than that without UV-ozone treatment, and the device with 30 min of UV-treatment had the best PCE of 17.17%. **Figure S7** shows the PCE histogram of PSCs based on $Ti_3C_2T_x$ film treated by UV-ozone for different time periods, which displays small standard deviation, indicating good reproducibility of devices.

Previously, $Ti_3C_2T_x$ has been demonstrated to be a metallic material, it has also been reported that its properties are strongly dependent on the surface chemistry and intercalated species.[28] We believe that in the case where the $Ti_3C_2T_x$ worked as ETL without UV-ozone treatment in PSCs, there would be significant current recombination , leading to low J_{sc}, FF. In fact, because of the metallic nature of $Ti_3C_2T_x$, it was expected that the cells might easily get short-circuited. However, it was interesting and surprising to find the $Ti_3C_2T_x$ treated with UV-ozone worked so well as ETL, blocking the holes at its interface with perovskite, which resulted in PCE as 17.17%. This indicated that $Ti_3C_2T_x$ after UV-ozone treatment, possesses more oxide-like surface termination, rendering it suitable as ETL and improving the interface

properties of $Ti_3C_2T_x$/perovskite. Moreover, because of the downward shift of the work function, the treatment made the layer of $Ti_3C_2T_x$ more appropriate to transmit electrons and reduce current recombination, leading to the rise of J_{sc} from 15.87 to 22.99 mA cm^{-2} and FF from 0.40 to 0.70.

The external quantum efficiency (EQE) spectra and integrated currents calculated for ETLs with different time of UV-ozone treatment (Figure 4e) are in line with the changes in J_{sc}. The integrated current density from EQE curves for the device of pristine $Ti_3C_2T_x$ without UV-ozone treatment is 14.91 mA cm^{-2}. A great increase of integrated current density is achieved by the UV-ozone treatment of the $Ti_3C_2T_x$ film, specifically it was increased to 19.29 mA cm^{-2} for the device after 10 min UV-ozone treatment and 20.40 mA cm^{-2} after 60 min UV-ozone treatment, while that of the best device with 30 min UV-ozone treatment was 20.22 mA cm^{-2}. The deviation between integrated current from EQE patterns and the actual measured J_{sc} values (Table 1) is about 10%, indicating good accuracy of the *J-V* obtained values. Besides, the hysteresis of reverse and forward scans of *J-V* curves is reduced from 49.6% for the device based on pristine $Ti_3C_2T_x$ to 27.1% for that based on $Ti_3C_2T_x$ with 30 min UV-ozone treatment (**Figure S8**).

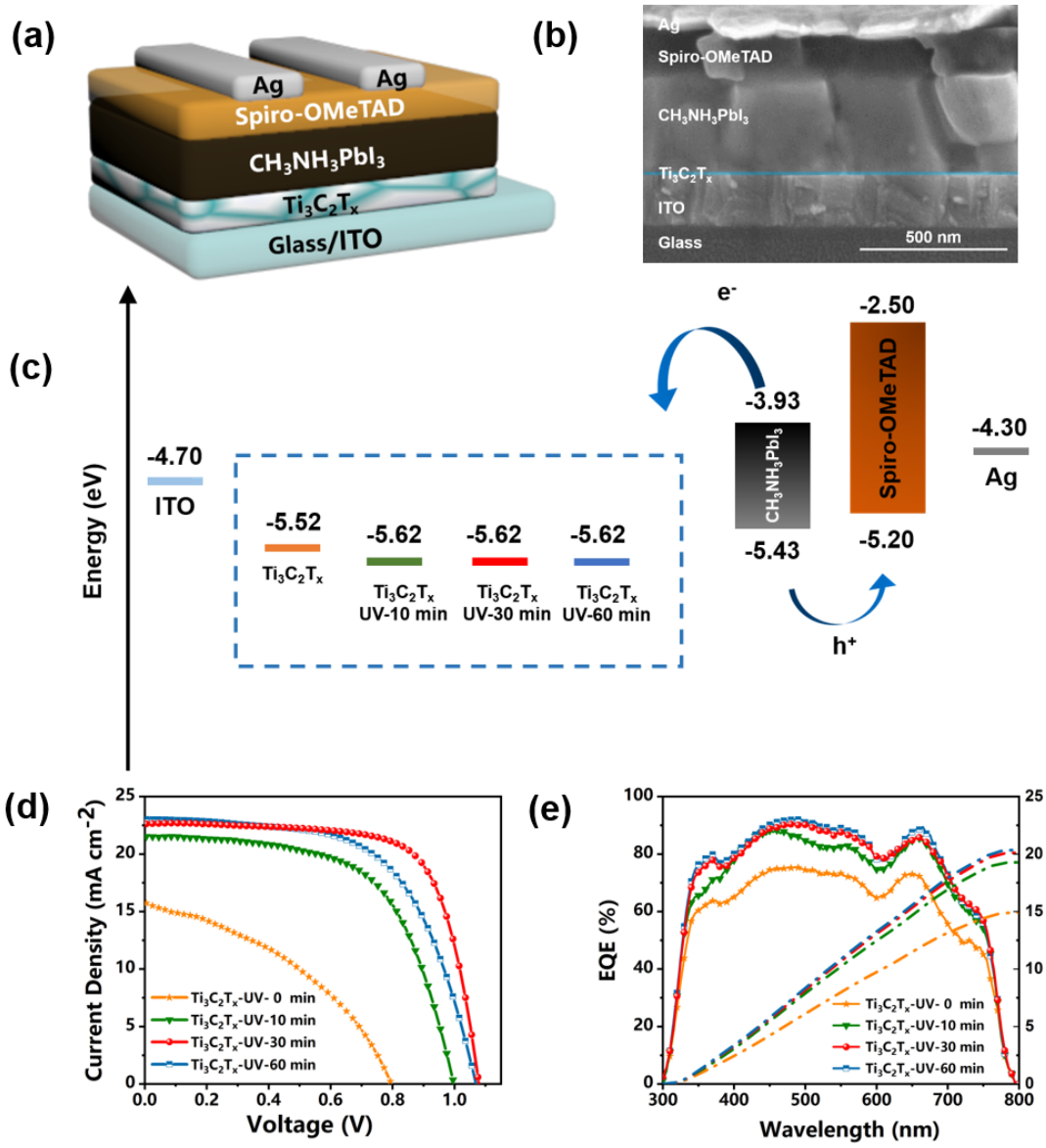

Figure 4. (a) Device architecture of ITO/ETL/$CH_3NH_3PbI_3$/Spiro-OMeTAD/Ag based on $Ti_3C_2T_x$ with/without UV-ozone treatment as ETL, (b) cross-sectional SEM image of the PSC device, (c) schematic energy-level diagram of each layer, (d) *J-V* curves of PSCs based on $Ti_3C_2T_x$ with UV-ozone treatment for different time as ETL under AM 1.5 G simulated illumination, and (e) their EQE spectra and the corresponding integrated current densities.

Table 1. The photovoltaic performance parameters of PSCs based on ETLs under different

conditions.

ETL	V_{oc} (V)	J_{sc} (mA cm^{-2})	FF (%)	PCE (%)
$Ti_3C_2T_x$-UV-0 min	0.80	15.87	40	5.00
$Ti_3C_2T_x$-UV-10 min	1.00	21.42	61	13.06
$Ti_3C_2T_x$-UV-30 min	1.08	22.63	70	17.17
$Ti_3C_2T_x$-UV-60 min	1.07	22.99	60	14.84

To understand the variations in FF, which is related to charge collection and conductivity, determined by interfacial charge transfer, electrochemical impedance spectroscopy (EIS) characterization was applied to the devices with the architecture of ITO/ $Ti_3C_2T_x$ (with or without UV-ozone)/$CH_3NH_3PbI_3$/Spiro-OMeTAD/Ag, at 0 V relative to the open-circuit potential with the frequency ranging from 1 MHz to 10 Hz under the standard AM 1.5 G (100 mW cm^{-2}) simulated sunlight illumination. **Figure 5**a provides the Nyquist plots of the four devices and the equivalent circuit model that was used to fit the experimental data. The fitted parameters are listed in Table S1. R_1 is the series resistance largely associated with external wires and the ITO substrate. The observed semi-circle represents the interfacial charge transfer resistance (R_2) and interfacial capacitance (C) at the interface of ETL/perovskite. The values of R_2 follow the order of $Ti_3C_2T_x$-UV-0 min > $Ti_3C_2T_x$-UV-10 min > $Ti_3C_2T_x$-UV-60 min > $Ti_3C_2T_x$-UV-30 min. PSCs based on $Ti_3C_2T_x$ with UV-ozone treatment have lower R_2 compared with that based on $Ti_3C_2T_x$ without UV-ozone treatment. The device with 30 min UV-ozone treated $Ti_3C_2T_x$ has the smallest R_2 of 27.86 Ω, indicating the lowest charge transfer resistance and the highest electrons collection at the interface, thus leading to the best

FF, which is in good agreement with *J-V* results.

Electron mobility values of the $Ti_3C_2T_x$ with or without UV-ozone treatment were measured by the method of space charge-limited current (SCLC) on the devices with electron-only structure of ITO/SnO_2/ETL/BCP/Ag under dark (**Figure S9**). There was no obvious change of SCLC with the processing time of UV-ozone treatment for $Ti_3C_2T_x$. The highest electron mobility was determined as 3.83×10^{-5} cm^2 V^{-1} s^{-1} for $Ti_3C_2T_x$ after 60 min UV-ozone treatment, while the pristine $Ti_3C_2T_x$ was 2.35×10^{-5} cm^2 V^{-1} s^{-1} and the $Ti_3C_2T_x$ after 10 min UV-ozone treatment was 2.72×10^{-5} cm^2 V^{-1} s^{-1}. The electron mobility of $Ti_3C_2T_x$ after 30 min UV-ozone treatment that gave the best PCE, was determined to be 3.03×10^{-5} cm^2 V^{-1} s^{-1}, which is about twenty times higher than that of TiO_2.[29] The mobility results effectively explain the improvement in J_{sc} and FF values in the device based on UV-ozone treated $Ti_3C_2T_x$ compared to the one based on non-treated $Ti_3C_2T_x$. Moreover, although the mobility of $Ti_3C_2T_x$ after 30 min UV-ozone treatment is a little lower than that after 60 min treatment, the resulting device performance is better. This could be explained by the lower series resistance and interfacial charge transfer resistance of the resulting device.

In addition to enhancement in the device performance, UV-ozone treatment on $Ti_3C_2T_x$ also contributed to the device stability, as displayed in Figure 5b. The devices were placed in ambient air (25 ^oC, relative humidity$\approx$20%) without encapsulation and tested under one sun illumination conditions (Figure 5b). The efficiency of pristine $Ti_3C_2T_x$ -based PSC reduced to 30% of its initial value within 384 h, while the device based on $Ti_3C_2T_x$ with 30 min UV-ozone treatment exhibited good stability up to 800 h by retaining about 70% of the

initial PCE after 800 h of storage. This reveals that appropriate UV-ozone treatment of the $Ti_3C_2T_x$ improves the device stability significantly. Although it is not very clear how the UV-ozone treated $Ti_3C_2T_x$ ETL improves stability, such dependence of performance deterioration of cells on different ETLs have been observed in several independent studies.[30] For instance, 2D materials like MoS_2 and WS_2 based perovskite solar cells with PCEs of 14.35 % and 15.00 % respectivelyhave been found to retain 78 % and 72 % of their PCEs up to 56 days in glovebox.[31] Yin *et al.* used TiS_2 as an ETL for planar perovskite solar cells to obtain a PCE of 17.37 % , which was comparable to that of the TiO_2 based reference device (17.07 %). Here, they found that TiS_2 ETL retained about 90 % of PCE under UV irradiation (10 mW cm^{-2}) in ambient atmosphere for 50 h while PCE of TiO_2 ETL based cell degraded by 44 % under same conditions.[32] We believe, the mechanism by which stability of the cells varies with different ETLs is very specific to the kind of materials used as ETL. Nonetheless, in our case here, the UV-ozone tretaed $Ti_3C_2T_x$ certainly shows improvement in stability. A detailed investigation of chemical and physical nature of the interface between perovskite and $T_3C_2T_x$ is needed to understand how exactly the UV-ozone treatment contributes to enhanced stability. In addition, we are certain that the stability could be improved further by combining the present system with other techniques, such as insertion of organic crosslinkers into perovskites, passivation of perovskite layer, and by selecting all-inorganic perovskite instead of hybrid-perovskites, which are indeed included in our future studies.[33]

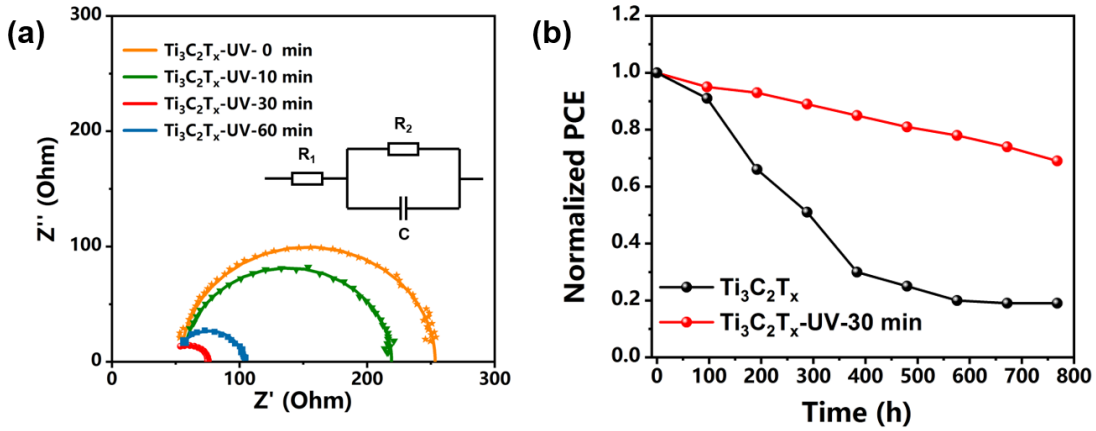

Figure 5. (a) Nyquist plots of the PSCs with $Ti_3C_2T_x$ after UV-ozone treatment for 0, 10, 30, and 60 min as ETLs under one sun illumination, where the scattered points are experimental data and the solid lines are the fitted curves according to the equivalent circuit. (b) The stability results of PSCs based on pristine $Ti_3C_2T_x$ and $Ti_3C_2T_x$ after 30 min UV-ozone treatment as ETLs in ambient air (relative humidity≈20%) without encapsulation at 25 °C.

3. Conclusion

2D $Ti_3C_2T_x$ films with flat and uniform surface were prepared by spin-coating and employed as electron transport layers for low-temperature processed planar PSCs with an architecture of ITO/ETL/$CH_3NH_3PbI_3$/Spiro-OMeTAD/Ag. UV-ozone treatment for different times were examined on the $Ti_3C_2T_x$ films to take advantage of the tunable optoelectronic properties of MXenes. A high PCE of 17.17% was achieved using 30 min UV-ozone treated $Ti_3C_2T_x$ as the ETL, highlighting the potential application of MXenes toward the development of low-cost and efficient solar cells. The greatly improved PCE originated from the additional oxide-like Ti-O bonds on the surface of $Ti_3C_2T_x$ ($Ti_3C_2O_2$) induced by

appropriate UV-ozone treatment, which improves the interface properties of $Ti_3C_2T_x$/perovskite and makes $Ti_3C_2T_x$ suitable as ETL for PSCs, thus led to much better J_{sc}, V_{oc} and FF, as evidenced by space charge-limited current and electrochemical impedance spectroscopy results. This work demonstrates the potential use of MXenes in solar cells. Moreover, the solution-processed MXene ETL can also be used in flexible photovoltaic devices.

4. Experimental Section

Materials: Lead iodide (PbI_2, >99.99%), methylammonium iodide (CH_3NH_3I, >99.5%) and lithium-bis (trifluoromethanesulfonyl) imide (Li-TFSI, >99%) were purchased from Xian Polymer Light Technology Corp. 2,2',7,7'-tetrakis-(*N,N*-di-*p*-methoxyphenylamino)-9,9'-spirobifluorene (Spiro-OMeTAD, >99.8%), 4-tert-butyl pyridine (tBP, 96%) and ultra-dry anhydrous *N,N*-dimethylformamide (DMF, 99.8%) were purchased from Sigma Aldrich. Dimethyl sulfoxide (DMSO, 99.7%) was obtained from Beijing Infinity Scientific (INFI). For MAX phase synthesis, titanium powder and aluminum powder were purchased from Aladdin. Graphite was purchased from Sigma Aldrich.

Preparation of $Ti_3C_2T_x$ MXene hydrocolloid: First, 7.368 g of titanium powder, 1.523 g of aluminum powder and 1.109 g of graphite were mixed together uniformly, then sintered at 1650°C for 2 hours under argon for preparing Ti_3AlC_2 MAX phase. The Ti_3AlC_2 MAX powder was grinded using mortar-pestle to pass through 400-mesh sieve and added into 12 M LiF/9 M HCl solution at room temperature. Briefly, 1.6 g LiF was added to 20 mL 9 M HCl under continuous stirring for several minutes. Then 1.0 g Ti_3AlC_2 MAX powder was gradually added (about 5 min) to the etchant solution and continuously etched for 24 h at

room temperature. When it was finished, the acidic mixture was washed with deionized water by repeated centrifugation (5 min per cycle at 8000 rpm). The supernatant was poured out and replaced by new deionized water after each cycle until the pH of mixture over 5. Finally, the slurry was placed in ultrasound for 10 min and centrifuged at 3500 rpm for 1 h. The colloid supernatant solution with $Ti_3C_2T_x$ nanosheets was obtained. To confirm its concentration, 10 mL of $Ti_3C_2T_x$ dispersion was filtered over a cellulose membrane (0.22 μm pore size). After drying and weighing the peeled-off $Ti_3C_2T_x$ film, the concentration of $Ti_3C_2T_x$ was determined to be 3 mg mL^{-1}.

Preparation of $Ti_3C_2T_x$ MXene films: By adding deionized water to $Ti_3C_2T_x$ dispersion (3 mg mL^{-1}), the $Ti_3C_2T_x$ colloid with lower concentration of 1 mg mL^{-1} was obtained. After softly shaking, the $Ti_3C_2T_x$ nanosheets would disperse well. $Ti_3C_2T_x$ MXene films were prepared by spin-coating 80 μL of colloids at 2500 rpm for 60 s onto the ITO substrates in air, followed by UV-ozone treatment of different time.

Device fabrication: The pre-patterned ITO were cleaned by detergent, deionized water, acetone, alcohol, and isopropanol in ultrasonic bath for 30 min respectively, then treated with UV ozone for 30 min. The ETL was prepared via spin-coating $Ti_3C_2T_x$ hydrocolloid onto the ITO substrates at 2500 rpm for 60 s in air, followed by the UV ozone treatment for 10, 30 and 60 min in sequence. Then the samples were moved into a glovebox filled with argon, where a perovskite ($CH_3NH_3PbI_3$) precursor solution was prepared by mixing 1.3 M (242 mg) PbI_2 and 1.3 M (83 mg) CH_3NH_3I in 408 μL DMF/DMSO (4:1 volume ratio) for more than 60 min. The perovskite layer was prepared by spin-coating its precursor solution (45 μL) at 5000 rpm for 30 s onto the ETL, and injecting chlorobenzene (350 μL) quickly onto the film in 5 s during the spin-coating process. The obtained film was then heated at 100 °C for 10 min. The hole transport material, Spiro-OMeTAD, was dissolved in chlorobenzene (80 mg mL^{-1}) and

stirred for 20 min. Then 10.5 mL of tBP and 15.5 mL of a Li-TFSI solution (510 mg Li-TFSI/1 mL acetonitrile) were added into Spiro-OMeTAD solution. After 5 minutes of stirring, 25 μL of solution was spin-coated at 4000 rpm for 30 s onto the $CH_3NH_3PbI_3$ layer. The samples were kept in the dark at room temperature overnight in dry air. Finally, the Ag electrode of 60 nm thickness was thermally evaporated on the top of Spiro-OMeTAD to assemble a complete PSC device.

Thin film characterization: UV-ozone treatment was employed by BZS250GF-TS UV-ozone cleaner. UV/Vis absorption spectra of ETLs on the glass were recorded using a Shimadzu UV-1900 spectrophotometer over the 300–900 nm wavelength range. The XRD patterns of $Ti_3C_2T_x$ with/without UV-ozone treatment coated on glass were recorded on Brucker D8 X-ray diffractometer with CuKα radiation (λ = 1.5418 Å) at 25 °C. The data was collected with a 0.02° step size (2θ) for 0.2 s. XPS measurements were also performed using ThermoFischer ESCALAB 250Xi. A field emission scanning electron microscope (Hitachi SU8000) was used to acquire top-view and cross-sectional SEM images.

Device characterization: The *J-V* characteristics of perovskite solar cells were measured by a Keithley 2400 source meter measurement system with an AM 1.5G filter at an illumination intensity of 100 mW cm^{-2}, as calibrated by a reference monocrystalline silicon solar cell (91150 V Oriel Instruments). The effective area of the cells was confirmed to be 0.04 cm^2 using a non-reflective metal mask. The EQE spectra were measured in air under short-circuit conditions using SOFN 7-SCSpecIII equipped with a 100 W Xe arc lamp, a filter wheel, and a monochromator. Monochromatic light was chopped at a frequency of 80 Hz and photocurrents were measured using a lock-in amplifier. The setup was calibrated using a certified silicon reference diode of known spectral response. The EIS measurements on the devices were carried out by a VSP multi-channel potentiostat (Biologic, France), under the

standard AM 1.5G (100 mW cm^{-2}) simulated sunlight illumination at open-circuit potential with the frequency ranging between 1 MHz and 10 Hz. Z-View Analyst software was used to model the Nyquist plots obtained from the impedance measurements.

Supporting Information

SEM images, XPS analysis, work functions results, optoelectronic parameters of $Ti_3C_2T_x$ with or without UV-ozone treatment, device reproducibility results, SCLC results and EIS fitting parameters. This material is available from website at http://..... or from the author.

Conflict of Interest

The authors declare no conflict of interest.

Acknowledgements

This work was supported by the National Natural Science Foundation of China (No. 1157411 1 to X.-F. W.) and "The Fundamental Research Funds for the Central Universities".

References

[1] A. Kojima, K. Teshima, Y. Shirai, T. Miyasaka, *J. Am. Chem. Soc.* **2009**, 131, 6050.

[2] J. Burschka, N. Pellet, S. J. Moon, R. Humphry-Baker, P. Gao, M. K. Nazeeruddin, M. Gratzel, *Nature* **2013**, 499, 316.

[3] a) S. D. Stranks, G. E. Eperon, G. Giulia, M. Christopher, M. J. P. Alcocer, L. Tomas, L. M. Herz, P. Annamaria, H. J. Snaith, *Science* **2013**, 342, 341; b) Y. Li, L. Meng, Y. M. Yang, G. Xu, Z. Hong, Q. Chen, J. You, G. Li, Y. Yang, Y. Li, *Nat. Commun.* **2016**, 7, 10214; c) Y. Liu, Y. Zhang, Z. Yang, D. Yang, X. Ren, L. Pang, S. F. Liu, *Adv. Mater.* **2016**, 28, 9204; d) P. P. Boix, K. Nonomura, N. Mathews, S. G. Mhaisalkar, *Mater. Today* **2014**, 17, 16; e) T. Miyasaka, *Chem. Lett.* **2015**, 44, 720; f) M. Liu, M.

B. Johnston, H. J. Snaith, *Nature* **2013**, 501, 395; g) Q. Ou, Y. Zhang, Z. Wang, J. A. Yuwono, R. Wang, Z. Dai, W. Li, C. Zheng, Z. Q. Xu, X. Qi, S. Duhm, N. V. Medhekar, H. Zhang, Q. Bao, *Adv. Mater.* **2018**, 30, e1705792.

[4] E. Aydin, M. De Bastiani, S. De Wolf, *Adv. Mater.* **2019**, DOI: 10.1002/adma.2019004281900428.

[5] H. Tsai, W. Nie, J. C. Blancon, C. C. Stoumpos, R. Asadpour, B. Harutyunyan, A. J. Neukirch, R. Verduzco, J. J. Crochet, S. Tretiak, L. Pedesseau, J. Even, M. A. Alam, G. Gupta, J. Lou, P. M. Ajayan, M. J. Bedzyk, M. G. Kanatzidis, *Nature* **2016**, 536, 312.

[6] a) J. Song, E. Zheng, J. Bian, X. F. Wang, W. Tian, Y. Sanehira, T. Miyasaka, *J. Mater. Chem. A* **2015**, 3, 10837; b) G. E. Eperon, V. M. Burlakov, P. Docampo, A. Goriely, H. J. Snaith, *Adv. Funct. Mater.* **2014**, 24, 151.

[7] Q. Chen, H. Zhou, Z. Hong, S. Luo, H. S. Duan, H. H. Wang, Y. Liu, G. Li, Y. Yang, *J. Am. Chem. Soc.* **2014**, 136, 622.

[8] T. Singh, S. Öz, A. Sasinska, R. Frohnhoven, S. Mathur, T. Miyasaka, *Adv. Funct. Mater.* **2018**, 28, 1706287.

[9] Y. Numata, R. Ishikawa, Y. Sanehira, A. Kogo, H. Shirai, T. Miyasaka, *J. Mater. Chem. A* **2018**, 6, 9583.

[10] J. T. W. Wang, J. M. Ball, E. M. Barea, A. Abate, J. A. Alexander-Webber, J. Huang, M. Saliba, I. n. Mora-Sero, J. Bisquert, H. J. Snaith, R. J. Nicholas, *Nano Lett.* **2014**, 14, 724.

[11] E. Jokar, Z. Y. Huang, S. Narra, C.-Y. Wang, V. Kattoor, C.-C. Chung, E. W. G. Diau, *Adv. Energy Mater.* **2018**, 8, 1701640.

[12] R. Singh, A. Giri, M. Pal, K. Thiyagarajan, J. Kwak, J. J. Lee, U. Jeong, K. Cho, *J. Mater. Chem. A* **2019**, 7, 7151.

[13] L. Lu, Z. Liang, L. Wu, Y. X. Chen, Y. Song, S. C. Dhanabalan, J. S. Ponraj, B. Dong, Y. Xiang, F. Xing, D. Fan, H. Zhang, *Laser. Photonics. Rev.* **2018**, 12, 1700221.

[14] a) M. Naguib, M. Kurtoglu, V. Presser, J. Lu, J. Niu, M. Heon, L. Hultman, Y. Gogotsi, M. W. Barsoum, *Adv. Mater.* **2011**, 23, 4248; b) M. Alhabeb, K. Maleski, B. Anasori, P. Lelyukh, L. Clark, S. Sin, Y. Gogotsi, *Chem. Mater.* **2017**, 29, 7633.

[15] X. Liang, A. Garsuch, L. F. Nazar, *Angew. Chem. Int. Ed. Engl.* **2015**, 54, 3907.

[16] Z. Ling, C. E. Ren, M. Q. Zhao, J. Yang, J. M. Giammarco, J. Qiu, M. W. Barsoum, Y. Gogotsi, *Proc. Natl. Acad. Sci. USA* **2014**, 111, 16676.

[17] Y. Sun, Y. Sun, X. Meng, Y. Gao, Y. Dall'Agnese, G. Chen, C. Dall'Agnese, X.-F. Wang, *Catal. Sci. Technol.* **2019**, 9, 310.

[18] G. Choi, F. Shahzad, Y.-M. Bahk, Y. M. Jhon, H. Park, M. Alhabeb, B. Anasori, D. S. Kim, C. M. Koo, Y. Gogotsi, M. Seo, *Adv. Opt. Mater.* **2018**, 6, 1701076.

[19] M. Ghidiu, M. R. Lukatskaya, M. Q. Zhao, Y. Gogotsi, M. W. Barsoum, *Nature* **2014**, 516, 78.

[20] a) C. Dall'Agnese, Y. Dall'Agnese, B. Anasori, W. Sugimoto, S. Mori, *New J. Chem.* **2018**, 42, 16446; b) Y. Chen, D. Wang, Y. Lin, X. Zou, T. Xie, *Electrochim. Acta.* **2019**, 316, 248.

[21] a) Z. Guo, L. Gao, Z. Xu, S. Teo, C. Zhang, Y. Kamata, S. Hayase, T. Ma, *Small* **2018**, 14, 1802738; b) L. Yang, Y. Dall'Agnese, K. Hantanasirisakul, C. E. Shuck, K. Maleski, M. Alhabeb, G. Chen, Y. Gao, Y. Sanehira, A. K. Jena, L. Shen, C.

Dall'Agnese, X. F. Wang, Y. Gogotsi, T. Miyasaka, *J. Mater. Chem. A* **2019**, 7, 5635.

[22] L. Zhou, Y. Zhang, Z. Zhuo, A. J. Neukirch, S. Tretiak, *J. Phys. Chem. Lett.* **2018**, 9, 6915.

[23] H. C. Fu, V. Ramalingam, H. Kim, C. H. Lin, X. Fang, H. N. Alshareef, J. H. He, *Adv. Energy Mater.* **2019**, 9, 1900180.

[24] Z. Yu, W. Feng, W. Lu, B. Li, H. Yao, K. Zeng, J. Ouyang, *J. Mater. Chem. A* **2019**, 7, 11160.

[25] a) Q. Tang, Z. Zhou, P. Shen, *J. Am. Chem. Soc.* **2012**, 134, 16909; b) P. Salles, D. Pinto, K. Hantanasirisakul, K. Maleski, C. E. Shuck, Y. Gogotsi, *Adv. Funct. Mater.* **2019**, 29, 1809223; c) X. Jiang, S. Liu, W. Liang, S. Luo, Z. He, Y. Ge, H. Wang, R. Cao, F. Zhang, Q. Wen, J. Li, Q. Bao, D. Fan, H. Zhang, *Laser. Photonics. Rev.* **2017**, 12, 1700229.

[26] X. Li, S. M. Dai, P. Zhu, L. L. Deng, S. Y. Xie, Q. Cui, H. Chen, N. Wang, H. Lin, *ACS. Appl. Mater. Interfaces* **2016**, 8, 21358.

[27] J. Pang, R. G. Mendes, A. Bachmatiuk, L. Zhao, H. Q. Ta, T. Gemming, H. Liu, Z. Liu, M. H. Rummeli, *Chem. Soc. Rev.* **2019**, 48, 72.

[28] a) T. Schultz, N. C. Frey, K. Hantanasirisakul, S. Park, S. J. May, V. B. Shenoy, Y. Gogotsi, N. Koch, *Chem. Mater.* **2019**, DOI: 10.1021/acs.chemmater.9b00414; b) J. L. Hart, K. Hantanasirisakul, A. C. Lang, B. Anasori, D. Pinto, Y. Pivak, J. T. van Omme, S. J. May, Y. Gogotsi, M. L. Taheri, *Nat. Commun.* **2019**, 10, 522.

[29] J. H. Heo, M. S. You, M. H. Chang, W. Yin, T. K. Ahn, S. J. Lee, S. J. Sung, D. H. Kim, S. H. Im, *Nano Energy* **2015**, 15, 530.

[30] a) S. Rafique, N. A. Roslan, S. M. Abdullah, L. Li, A. Supangat, A. Jilani, M. Iwamoto, *Org. Electron.* **2019**, 66, 32; b) Y. Zhang, C. K. Lim, Z. Dai, G. Yu, J. W. Haus, H. Zhang, P. N. Prasad, *Phys. Rep.* **2019**, 795, 1.

[31] P. Huang, Z. Wang, Y. Liu, K. Zhang, L. Yuan, Y. Zhou, B. Song, Y. Li, *ACS. Appl. Mater. Interfaces* **2017**, 9, 25323.

[32] G. Yin, H. Zhao, J. Feng, J. Sun, J. Yan, Z. Liu, S. Lin, S. Liu, *J. Mater. Chem. A* **2018**, 6, 9132.

[33] J. Song, E. Zheng, X. F. Wang, W. Tian, T. Miyasaka, *Sol. Energ. Mat. Sol. C.* **2016**, 144, 623.